

© IEEE. Personal use of this material is permitted. However, permission to reprint/republish this material for advertising or promotional purposes or for creating new collective works for resale or redistribution to servers or lists, or to reuse any copyrighted component of this work in other works must be obtained from the IEEE.

This material is presented to ensure timely dissemination of scholarly and technical work. Copyright and all rights therein are retained by authors or by other copyright holders. All persons copying this information are expected to adhere to the terms and constraints invoked by each author's copyright. In most cases, these works may not be reposted without the explicit permission of the copyright holder.

COMBINING GAUSSIAN MARKOV RANDOM FIELDS WITH THE DISCRETE WAVELET TRANSFORM FOR ENDOSCOPIC IMAGE CLASSIFICATION

M. Häfner¹, A. Gangl¹, M. Liedlgruber^{2,*}, A. Uhl^{2,*}, A. Vécsei³, and F. Wrba⁴

¹ Department of Gastroenterology and Hepatology, Medical University of Vienna, Austria

² Department of Computer Sciences, Salzburg University, Austria

³ St. Anna Children's Hospital, Vienna, Austria

⁴ Department of Clinical Pathology, Medical University of Vienna, Austria

* Corresponding author e-mail: {mliedl, uhl}@cosy.sbg.ac.at

ABSTRACT

In this work we present a method for automated classification of endoscopic images according to the pit pattern classification scheme. Images taken during colonoscopy are transformed to the wavelet domain using the pyramidal discrete wavelet transform. Then, Gaussian Markov random fields are used to extract features from the resulting wavelet coefficients. Finally, these features are used for a classification using the k-NN classifier and the Bayes classifier.

To enhance the classification results feature subset selection is used to reduce the dimensionality of the features. Apart from that, directional neighborhoods for the Markov random fields are introduced. These are exploiting the orientation of the details within the wavelet detail subbands with the goal of further improving the classification performance.

The experimental results show that an automated classification using the presented method is feasible.

Index Terms— Colonoscopy, colon cancer, wavelet transform, markov random fields, classification

1. INTRODUCTION

Today, the third most common malignant disease in western countries is colon cancer. Therefore a regular colon examination is recommended, especially for people at an age of 50 years and older. Such a diagnosis can be done for example by *colonoscopy*, which is currently the best test available to identify colon cancer.

Colonoscopy is a medical procedure which allows a physician to investigate the inside of the colon. This is done by using a colonoscope, a flexible instrument equipped with a CCD chip for visualization of the organ and controlled by the physician. In case a lesion is detected, tissue samples can be taken and relevant lesions can be removed, avoiding thus surgery.

Modern colonoscopes are able to take pictures from inside the colon, which allows a physician to review the results of a colonoscopy to document the growth and spreading of an eventual tumorous lesion. Apart from that the images might be used for computer-assisted analysis with the goal of detecting tumorous lesions which is the aim of this work.

To get images which are as detailed as possible a special endoscope (*magnifying endoscope*) is used. A magnifying endoscope represents a significant advance in colonoscopic diagnosis as it provides images which are up to 150-fold magnified. Images taken with this type of endoscope uncover the fine surface structure of the mucosa as well as small lesions.

In this work we use *Gaussian Markov random fields* in conjunction with the pyramidal discrete wavelet transform (DWT) for an automated classification of visual data acquired by a magnifying colonoscope corresponding to different types of lesions. In Section 2 we review the classification of pit patterns of the colonic mucosa. Section 3 gives an introduction to Markov random fields and describes the types of features extracted from the wavelet subbands resulting from the DWT by applying a Gaussian Markov random field to the coefficients. In Section 4 we introduce a custom set of scalable neighborhoods for the GMRFs. Experimental results and configuration details of the classification system proposed in this work are presented and discussed in Section 5. Section 6 concludes the paper.

2. PIT PATTERN CLASSIFICATION

Polyps of the colon are a frequent finding and are usually divided into metaplastic, adenomatous, and malignant. As resection of all polyps is time-consuming, it is imperative that those polyps which warrant endoscopic resection can be distinguished: polypectomy of metaplastic lesions is unnecessary and removal of invasive cancer may be hazardous. For these reasons, assessing the malignant potential of lesions at the time of colonoscopy is important.

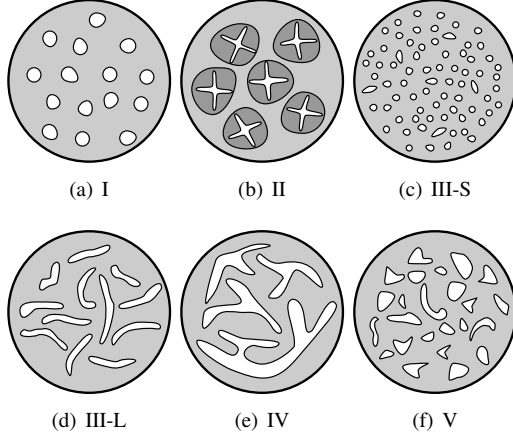


Fig. 1. Pit pattern classification according to Kudo et al.

To be able to differentiate between the different types of lesions a classification method is needed. The most commonly used classification system for distinguishing between non-neoplastic and neoplastic lesions in the colon is the pit pattern classification, originally reported by Kudo et al. [11, 12].

This system allows a differentiation between normal mucosa, hyperplastic lesions (non-neoplastic), adenomas (a pre-malignant condition), and malignant cancer based on the visual pattern of the mucosal surface. Hence, this classification scheme is a convenient tool to decide which lesions need not, which should and which most likely can not be removed endoscopically. The mucosal pattern as seen after dye staining and by using magnification endoscopy shows a high agreement with the histopathologic diagnosis.

As illustrated in Fig. 1, this classification differentiates between five main types according to the mucosal surface of the colon. Type III is divided into types III-S and III-L, designating the size of the pit structure. It has been suggested that type I and II pattern are characteristic of non-neoplastic lesions, type III and IV are found on adenomatous polyps, and type V are strongly suggestive of invasive carcinoma.

Lesions of type I and II are benign, representing the normal mucosa or hyperplastic tissue, and in fact are non-tumorous. Lesions of type III and IV in contrast represent lesions which are neoplastic. Type V lesions usually are highly indicative for cancer. Lesions of type I and II can be grouped into non-neoplastic lesions and lesions of type III to V can be grouped into neoplastic lesions. Thus a coarser grouping of lesions into two instead of six classes is possible too.

Using a magnifying colonoscope together with indigo carmine dye spraying, the mucosal crypt pattern on the surface of colonic lesions can be observed [12]. Several studies found a good correlation between the mucosal pit pattern and the histological findings, where especially techniques using magnifying colonoscopes led to excellent results [7].

As depicted in Fig. 1, pit pattern types I to IV can be characterized fairly well, while type V is a composition of un-

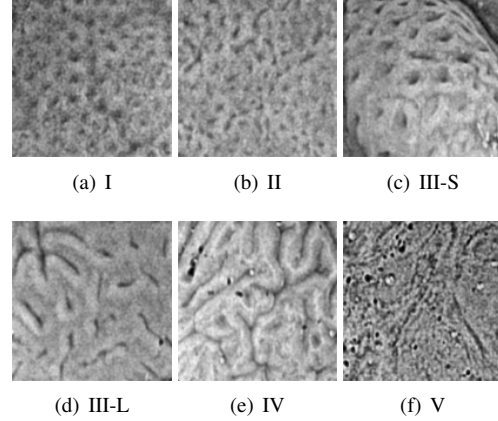


Fig. 2. Images showing the different types of pit pattern.

structured pits. At a first glance this classification scheme seems to be straightforward and easy to be applied. But it needs some experience and exercising to achieve fairly good results [6, 18]. This gets obvious from the example images shown in Fig. 2 (taken out of the training set used throughout this work).

3. MARKOV RANDOM FIELDS

Markov random fields (MRFs) allow the modeling of local characteristics in an image in terms of a stochastic process. In the past MRFs have already been used successfully for example for texture classification [2, 15, 14, 5, 20, 19], segmentation [17, 9, 1, 10], and texture synthesis [15].

When applying MRFs to problems in image processing a MRF is associated with a regular lattice $S = \{1, \dots, M\}$, where M is the number of pixels in the image and i is indexing the pixels of the image in a sequential order from top left to bottom right.

Apart from that a neighborhood is needed to express the local interactions between neighboring pixels. In literature there exist different definitions for neighborhoods of order n (e.g. [15, 4]). Throughout our experiments we used the homogeneous neighborhood defined in [4]. For this type a neighborhood of order n for a site i on the lattice S is defined as $N_i^n = \{i' : |i - i'| \leq n, i' \neq i\}$, where i' denotes a site belonging to the neighborhood and $|i - i'|$ denotes the euclidean distance between two sites i and i' . Fig. 3 shows two possible neighborhoods of this type. The set of all neighborhoods $N^n = \{N_i^n : i \in S\}$ is called a *neighborhood system*.

Furthermore, the lattice is associated with a family of random variables $F = \{F_1, \dots, F_M\}$ (also called *random field*) which describe the pixel values in the image. Each of these random variables F_i is associated with a site i and takes a valid pixel value $f_i \in L$ (where $L = \{1, \dots, W\}$ is the set of valid labels, e.g. the allowed luminance values for a pixel). Thus, the event $f = \{f_1, \dots, f_M\}$ represents one possible re-

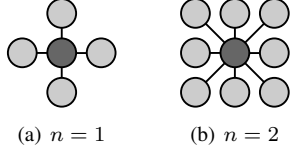


Fig. 3. Images showing two different neighborhoods of order 1 and 2 according to [4]. The dark-gray circles denote the center pixels which do not belong to the respective neighborhood.

alization of the MRF, also referred to as *configuration* (in our case, one possible image).

F along with a neighborhood system N^n constitutes a MRF on S if the following two properties hold:

$$P(f) > 0 \quad \forall f \in \mathbb{F} \quad (\text{Positivity})$$

$$P(f_i | f_{S-\{i\}}) = P(f_i | f_{N_i^n}) \quad (\text{Markovianity})$$

where $f_{S-\{i\}}$ denotes the set of all sites of the lattice S except site i , $\mathbb{F} = L^M$ denotes the set of all possible configurations, and $f_{N_i^n}$ denotes the set of pixel values at the sites in the neighborhood of i .

The positivity states that the probability for each possible image to occur must be greater than zero. The Markovianity states that the value of a pixel is only dependent on the pixel values in the respective neighborhood. This property is especially important since it allows the modeling of local interactions between neighboring pixels in terms of local conditional probabilities.

3.1. The Gaussian MRF model

This work is based on the so-called *auto-normal* Markov random field model, also known as the Gaussian MRF (GMRF) model [13, 15], with the local conditional probability defined as

$$P(f_i | f_{N_i^n}) = \frac{1}{\sqrt{2\pi\sigma^2}} \exp\left(-\frac{\left(f_i - \sum_{l=1}^C \alpha_l f_i^{(l)}\right)^2}{2\sigma^2}\right) \quad (1)$$

where α_l are the *Markov parameters*, $f_i^{(l)}$ is the sum of the pixel values contained within the l -th pair of sites in symmetric positions about a site i , and C denotes the number of these pairs (i.e. $C = |N_i^n|/2$).

To get the estimates $\hat{\alpha}_l$ of the Markov parameters we use the Least square parameter estimates [15, 2, 8]. Additionally we use the variance of the approximation error, which is defined as

$$\eta = \frac{1}{|S_I|} \sum_{i \in S_I} \left(f_i - \sum_{l=1}^C \hat{\alpha}_l f_i^{(l)}\right)^2 \quad (2)$$

where $S_I \subset S$ is the set of all interior sites in S whose complete set of neighbors lies inside the bounds of the image too and $\hat{\alpha}_l$ is the parameter estimate for the l -th pixel pair.

3.2. Feature extraction

Instead of performing the parameter estimation directly on the image data, we first transform the image to the wavelet domain using the pyramidal DWT. The motivation behind switching to the wavelet domain is that the optimal size of the GMRF neighborhood for a specific image class is not known at beforehand. Apart from that textures usually exhibit different characteristics at different resolutions. By exploiting the multiresolution property of the DWT a neighborhood of some fixed order is assumed to already capture texture characteristics at different resolutions.

A similar method has already been proposed in previous work [20, 19]. But while in [20, 19] the subbands are binarized, which results in an auto-logistic random field model, we use the unaltered wavelet coefficients as input for the MRF. Apart from that in [19] the parameters are combined with wavelet energy signatures acquired from the detail subbands to form the final feature vectors.

In our approach the parameters $\hat{\alpha}_l$ and η are estimated for each of the detail subbands, which results in $3m(C+1)$ parameters for one color channel (m denotes the maximum level of decomposition). The resulting feature vector for a color channel is of the form $\mathcal{S} = (f_1 \circ \dots \circ f_t)$, where \circ denotes the vector concatenation and $f_k = (\hat{\alpha}_{1,k}, \dots, \hat{\alpha}_{C,k}, \eta_k)$ is the feature vector part for the k -th subband ($\hat{\alpha}_{j,k}$ and η_k denote the parameters for the k -th subband). Since we use all color channels available the final feature vectors are of the form $\mathcal{F} = (\mathcal{S}_1 \circ \mathcal{S}_2 \circ \mathcal{S}_3)$, where \mathcal{S}_j denotes the feature vector for the j -th color channel.

3.3. Classification

For the classification task we compare two distinct classifiers, namely the k -Nearest Neighbor (k -NN) classifier and the Bayes classifier. The k -NN classifier assigns that class to an unknown image which dominates among the k nearest neighbors of the unknown image in feature space. The Bayes classifier, covered in more detail in [3], is a probabilistic classifier based on the Bayes theorem which assigns an unknown image to the most probable class it belongs to.

3.4. Feature subset selection

When estimating the parameters in the wavelet domain the length of the feature vectors is $3m$ times higher compared to the spatial domain (in the spatial domain one single GMRF is used for the whole image). This induces a higher computational demand in terms of the classifier training and the classification. Apart from that, since the feature vectors have different lengths compared to the spatial domain counterparts, the experimental results can not be compared directly.

As a consequence we use a feature subset selection algorithm to shorten the feature vectors from the wavelet domain to match the spatial domain lengths (for equal neighborhood

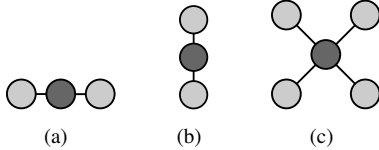


Fig. 4. The custom neighborhoods capturing the vertical (a), horizontal (b), and diagonal details (c) within the LH, HL, and HH detail subbands, respectively.

orders). There exist various different algorithms from which we chose the *sequential floating forward search* (SFFS) [16] due to its superior performance in terms of running time and since it delivers a nearly optimal feature subset.

Basically this algorithm first adds the best feature to the candidate set (in terms of some criterion function, e.g. the fisher criterion). Then the algorithm tests if one or more of the worst features may be removed according to the criterion function. If the loss incurred by removing a feature candidate is lower than the gain of the previous add operation, the feature is dropped and another possible feature for removal is tested. Otherwise the algorithm returns to the adding step. These steps are repeated until the desired target dimensionality is reached. In our case the target dimensionality D_T corresponds to the dimensionality of the feature vectors within the spatial domain.

4. CUSTOM NEIGHBORHOODS

In addition to the Geman-type neighborhood we also carried out experiments with custom neighborhoods. Motivated by the fact that the different detail subbands resulting from the DWT contain details of different orientations, we use differently orientated neighborhoods for each detail subband type (HL, LH, and HH). These custom neighborhoods are depicted in Fig. 4. Again we have an order parameter which now specifies the maximum extent of such a neighborhood in pixels in the respective direction (measured from the center pixel of the neighborhood).

The feature extraction process and subsequent classification are carried out as described above. The target dimension for the feature subset selection is based on a reference neighborhood of Geman-type (as used for the spatial domain approach). The order of the reference neighborhood is chosen to correspond with the order of the respective custom neighborhoods.

5. EXPERIMENTS

5.1. Settings

The image database used throughout our experiments consists of 484 images acquired in 2005 and 2006 at the Department of Gastroenterology and Hepatology (Medical University of

	I	II	III-S	III-L	IV	V
2 classes	198		286			
6 classes	126	72	18	62	146	60

Table 1. Number of images per class used in our experiments.

Vienna) using a zoom-colonoscope (Olympus Evis Exera CF-Q160ZI/L) with a magnification factor set to 150.

Lesions found during colonoscopy have been examined after application of dye-spraying with indigocarmine as routinely performed in colonoscopy. Biopsies or mucosal resection have been performed in order to get a histopathological diagnosis. Biopsies have been taken from type I, II, and type V lesions, as those lesions need not to be removed or cannot be removed endoscopically. Type III and IV lesions have been removed endoscopically. Out of all acquired images, histopathological classification resulted in 198 non-neoplastic and 286 neoplastic cases. The detailed classification results, which are used as ground truth for our experiments, are shown in Table 1.

Using leave-one-out cross-validation, 483 out of 484 images are used as training set. The remaining image is then classified. This process is repeated for each image.

To show the advantage of estimating the Markov parameters in the wavelet domain, we carried out experiments in the wavelet domain as well as in the spatial domain. In both cases all color channels of the RGB color space have been used for parameter estimation. Prior to feature extraction we first applied an averaging filter for smoothing, followed by enhancing the contrast using CLAHE [21]. The wavelet-based results have been obtained by using the Haar wavelet with a two-level wavelet decomposition.

5.2. Results

As we can see from Table 2, estimating the Markov parameters in the wavelet domain in the 2-classes case clearly yields better results. In the case of the k-NN classifier we achieve an overall classification rate of 92,6 % in the wavelet domain (without SFFS) compared to 83,3 % in the spatial domain. The Bayes classifier shows the desired behavior behind the idea of switching to the wavelet domain by showing the best result at $n = 8$ instead of $n = 13$ in the spatial domain. But the top result of 92,8 % in the wavelet domain (with SFFS) is only slightly higher compared to 92,1 % in the spatial domain.

In the 6-classes case estimating the parameters in the wavelet domain yields a considerable improvement in the case of the k-NN classifier with a top result of 80,0 % (without SFFS) compared to 63,2 % in the spatial domain. But when using the Bayes classifier we get a top result of 73,8 % in the wavelet domain (with SFFS) compared to the spatial domain top result of 77,9 %, which is a considerable loss.

For custom neighborhoods the picture is very similar (ta-

n	D_T	D_O	k-NN			Bayes		
			S	W	R	S	W	R
1	9	54	72,7	88,2	86,6	88,4	91,7	89,7
2	15	90	80,6	90,1	86,8	86,0	91,9	89,9
4	21	126	74,4	91,5	88,0	87,6	86,0	91,5
5	33	198	81,6	91,7	88,4	89,3	83,9	90,5
8	39	234	83,3	92,6	90,9	90,1	69,2	92,8
9	45	270	80,8	91,7	89,5	90,7	42,8	91,5
10	57	342	81,0	91,3	88,0	89,9	59,1	87,4
13	69	414	80,2	91,7	89,7	92,1	59,1	86,8
16	75	450	80,6	90,9	88,8	90,3	59,1	87,4

Table 2. Detailed overall classification rates in percent for different neighborhood orders n (2-classes). D_T and D_O denote the target dimension for SFFS and the original dimensionality in the wavelet domain, respectively. S, W, and R denote the spatial domain, the wavelet domain, and the wavelet domain with SFFS applied, respectively. The top results are shown in bold numbers.

n	D_T	D_O	k-NN			Bayes		
			S	W	R	S	W	R
1	9	54	44,8	70,0	66,9	64,7	53,9	64,3
2	15	90	57,2	75,6	69,2	70,7	48,1	67,6
4	21	126	55,2	79,1	72,5	77,9	53,5	73,8
5	33	198	62,8	79,5	73,1	71,5	30,2	66,5
8	39	234	63,2	80,0	74,0	69,6	30,2	63,2
9	45	270	60,5	78,7	72,9	65,7	30,2	59,9
10	57	342	62,6	78,3	74,8	50,0	30,2	50,8
13	69	414	62,2	77,5	74,2	49,2	30,2	50,2
16	75	450	62,0	77,3	75,4	46,3	30,2	48,8

Table 3. Detailed overall classification rates (6-classes).

bles 4 and 5). In the 2-classes case the highest overall classification result achieved with the k-NN classifier is considerably higher in the wavelet domain (without SFFS) with 95,7 % compared to 83,3 % in the spatial domain. The top result for the Bayes classifier is slightly higher with 92,8 % (without SFFS) compared to 92,1 % in the spatial domain. But $n = 2$ for the best result is considerably lower in the wavelet domain compared to $n = 13$ in the spatial domain.

In the 6-classes case (Table 3) switching to the wavelet domain yields a considerable improvement when using the k-NN classifier with a top result of 83,9 % (without SFFS) compared to 63,2 % in the spatial domain. The Bayes classifier achieves a top result of 76,0 % in the wavelet domain (with SFFS) compared to the spatial domain top result of 77,9 %.

5.3. Summary of results

When using the custom neighborhoods proposed the results in the wavelet domain are almost always higher compared to the results obtained using Geman neighborhoods. The im-

n	D_T	D_O	k-NN			Bayes		
			S	W	R	S	W	R
1	9	42	72,7	91,5	89,3	88,4	92,6	90,9
2	15	66	80,6	93,8	91,9	86,0	92,8	92,1
3	15	90	80,6	94,8	93,0	86,0	92,1	89,3
4	21	114	74,4	94,4	93,8	87,6	86,8	90,5
5	33	138	81,6	95,7	93,2	89,3	79,5	90,3
6	33	162	81,6	95,0	90,5	89,3	64,7	91,9
7	33	186	81,6	94,2	88,8	89,3	59,5	90,1
8	39	210	83,3	94,0	93,4	90,1	72,1	88,8
9	45	234	80,8	92,6	90,9	90,7	66,1	87,4
10	57	258	81,0	92,6	91,5	89,9	47,1	89,0
11	57	282	81,0	90,7	90,3	89,9	41,3	89,0
12	57	306	81,0	89,3	89,3	89,9	59,1	90,3
13	69	330	80,2	88,2	89,0	92,1	59,1	89,5
14	69	354	80,2	87,6	87,2	92,1	59,1	86,8
15	69	378	80,2	87,0	86,4	92,1	59,1	87,6

Table 4. Detailed overall classification rates for custom neighborhoods (2-classes).

provements are ranging from approximately 3 % to 12 % (6-classes case using the Bayes classifier). But as we can see from the results, in most cases still higher-order neighborhoods are needed, which induce a higher computational complexity for the parameter estimation process. As a result the feature vectors are rather high-dimensional, which results in a higher computational demand in terms of the classification process. Apart from that, although showing the best results with rather low dimensions, the results of the Bayes classifier are in general lower within the wavelet domain compared to the results of the k-NN classifier, which however in general yields worse classification results when using subset selection.

6. CONCLUSION

In this work we showed that the classification of endoscopic images according to the pit pattern scheme by using GM-RFs in the wavelet domain is feasible. By exploiting the multiresolution property of the wavelet transform we almost always achieve considerably higher classification accuracies compared to the results in the spatial domain. We also showed that by using differently orientated neighborhoods for the different subbands types we are able to achieve even higher classification results.

7. ACKNOWLEDGMENTS

This work is partially funded by the Austrian Science Fund (FWF) under Project No. L366-N15 and by the Austrian National Bank ‘‘Jubil umsfonds’’ Project No. 12514.

n	D_T	D_O	k-NN			Bayes		
			S	W	R	S	W	R
1	9	42	44,8	77,3	69,6	64,7	65,7	67,4
2	15	66	57,2	82,2	76,4	70,7	53,5	75,2
3	15	90	57,2	83,3	77,5	70,7	51,2	72,9
4	21	114	55,2	82,4	76,7	77,9	35,5	76,0
5	33	138	62,8	83,7	78,7	71,5	26,2	72,7
6	33	162	62,8	83,9	78,5	71,5	30,2	73,3
7	33	186	62,8	81,6	76,2	71,5	30,2	70,9
8	39	210	63,2	81,0	78,9	69,6	30,2	66,9
9	45	234	60,5	79,8	77,7	65,7	30,2	61,6
10	57	258	62,6	79,1	76,2	50,0	30,2	53,1
11	57	282	62,6	77,1	77,3	50,0	30,2	51,2
12	57	306	62,6	76,2	75,4	50,0	30,2	51,9
13	69	330	62,2	73,3	73,3	49,2	30,2	50,8
14	69	354	62,2	72,3	73,6	49,2	30,2	50,4
15	69	378	62,2	71,1	69,6	49,2	30,2	49,6

Table 5. Detailed overall classification rates for custom neighborhoods (6-classes).

References

- [1] M.G. Bello. A combined markov random field and wave-packet transform-based approach for image segmentation. *IEEE Transactions on Image Processing*, 3:834–846, 1994.
- [2] R. Chellappa and S. Chatterjee. Classification of textures using gaussian markov random fields. *IEEE Transactions on Acoustics, Speech, and Signal Processing*, 33:959–963, 1985.
- [3] K. Fukunaga. *Statistical Pattern Recognition*. Morgan Kaufmann, 2nd edition, 1990.
- [4] S. Geman and D. Geman. Stochastic relaxation, gibbs distributions, and the bayesian restoration of images. *IEEE Transactions on Pattern Analysis and Machine Intelligence*, 6:721–741, 1984.
- [5] O.J. Hernandez, J. Cook, M. Griffin, C. De Rama, and M. McGovern. Classification of color textures with random field models and neural networks. *Journal of Computer Science and Technology*, 5(3):16, October 2005.
- [6] D.P. Hurlstone. High-resolution magnification chromoendoscopy: Common problems encountered in “pit pattern” interpretation and correct classification of flat colorectal lesions. *American Journal of Gastroenterology*, 97:1069–1070, 2002.
- [7] D.P. Hurlstone et al. Efficacy of high magnification chromoscopic colonoscopy for the diagnosis of neoplasia in flat and depressed lesions of the colorectum: a prospective analysis. *Gut*, 53:284–290, 2004.
- [8] R. Kashyap and R. Chellappa. Estimation and choice of neighbors in spatial-interaction models of images. *IEEE Transactions on Information Theory*, 29:60–72, 1983.
- [9] Z. Kato and T.C. Pong. A markov random field image segmentation model for color textured images. *Image and Vision Computing*, 24(10):1103–1114, 2006.
- [10] S. Krishnamachari and R. Chellappa. Multiresolution gauss-markov random field models for texture segmentation. *IEEE Transactions on Image Processing*, 6:251–267, 1997.
- [11] S. Kudo et al. Colorectal tumorous and pit pattern. *Journal of Clinical Pathology*, 47:880–885, 1994.
- [12] S. Kudo et al. Diagnosis of colorectal tumorous lesions by magnifying endoscopy. *Gastrointestinal Endoscopy*, 44(1):8–14, July 1996.
- [13] S.Z. Li. *Markov Random Field Modeling in Image Analysis*. Springer, Berlin, 2001.
- [14] R. Paget, I.D. Longstaff, and B. Lovell. Texture classification using nonparametric markov random fields. In *Proceedings of the 13th International Conference on Digital Signal Processing (DSP’97)*, volume 1, pages 67–70, 1997.
- [15] M. Petrou and P.G. Sevilla. *Image Processing. Texture: Dealing with Texture*. Wiley John and Sons, 1st edition, 2006.
- [16] P. Pudil, J. Novovicova, and J. Kittler. Floating search methods in feature-selection. *Pattern Recognition Letters*, 15(11):1119–1125, November 1994.
- [17] T. Szirányi, J. Zerubia, L. Czúni, D. Geldreich, and Z. Kato. Image segmentation using markov random field model in fully parallel cellular network architectures. *Real-Time Imaging*, 6:195–211, 2000.
- [18] S. Tung, C. Wu, and M. Su. Magnifying colonoscopy in differentiating neoplastic from nonneoplastic colorectal lesions. *American Journal of Gastroenterology*, 96:2628–2632, 2001.
- [19] L. Wang, J. Liu, and S.Z. Li. MRMRF-based texture classification. In *Proceedings of Joint Conference on Information Science (JCIS’98)*, pages 226–229, 1998.
- [20] L. Wang, J. Liu, and S.Z. Li. Texture classification using wavelet decomposition with markov random field models. In *Proceedings of Fourteenth International Conference on Pattern Recognition.*, volume 2, pages 1613–1615, 1998.
- [21] K. Zuiderveld. Contrast limited adaptive histogram equalization. *Graphics Gems IV*, pages 474–485, 1994.